Contribution of surface energy to pH dependent underwater adhesion of an acrylic pressure sensitive adhesive

Preetika Karnal[1], Anushka Jha[1], Hanqi Wen[1], Stefan Gryska[3], Carlos Barrios[3,*], and Joelle Frechette.[1,2,*],

[1]Chemical and Biomolecular Engineering Department, [2] Hopkins Extreme Materials Institute, (HEMI), Johns Hopkins University, Baltimore MD 21218

[3]3M Company, 3M Center, Building 201-4N-01, St. Paul, MN, 55144-1000

ABSTRACT

Maintaining the underwater adhesive performance over a broad range of solution pH is challenging but necessary for many biomedical applications. Therefore, understanding how environmental conditions influence the mechanisms of bonding and debonding of pressure sensitive adhesives (PSAs) could provide guidelines for materials design. We investigate how the presence of acrylic acid co-monomer impacts the adhesion of a model PSA in aqueous environments of varying pH. The adhesives under investigation are poly(2-ethylhexyl acrylate), or poly(2-EHA), and poly(2-EHA) copolymerized with 5wt% acrylic acid, or poly(2-EHA-co-AA). We characterize bonding and debonding (adhesion) of the adhesives using probe tack measurements with a spherical hydrophobic glass probe. We analyze the performance of the two PSAs in air and in low ionic strength buffered aqueous solutions of pH3-pH11. We find that the presence of the acrylic acid co-monomer increases the cohesiveness of the PSA and leads to stronger adhesion under all conditions investigated. We also observe that the presence of the acrylic acid co-monomer imparts the PSA with a strong dependence of adhesion on the solution pH. Dynamic contact angle and zeta potential measurements support the hypothesis that deprotonation of the acrylic acid groups at higher pH causes the decrease in adhesion at higher pH. Rheological measurements do not show changes in the dynamic mechanical properties of the PSAs after exposure to solutions of pH3-pH11. Our measurements allow us to isolate the effect of the solution pH on the surface and bulk properties of the PSA. In the absence of the acrylic acid co-monomer, the bulk dissipation and the surface properties of the PSA are independent of the solution's pH.

* corresponding authors, jfrechette@jhu.edu and cabarrios@mmm.com

1. INTRODUCTION

A pressure sensitive adhesive (PSA) adheres to a surface once a light external pressure is applied, and can be designed to debond without leaving a residue on the surface[1]. Their simplicity and ease of use make PSAs ubiquitous in everyday life (for example consider Scotch® tape and Post-it® notes). In addition, PSAs are also present in electronics,[2-3] in the automotive industry,[4] and in modern medical items such as wound dressings and drug delivery patches[5]. Both the surface and bulk properties of a PSA determine its performance. The surface properties lead to an interfacial bond, for example through van der Waals forces, but the rate dependent viscoelastic dissipation in the bulk amplifies, by orders of magnitude, the energy required to detach the adhesive from the substrate. In fact, due to their viscous component some PSAs can sustain very large strains (>100%) prior to failure.[6] While the general mechanisms of bonding and debonding of PSAs in air are relatively well-established, there are only a limited number of scientific reports addressing how water, and more generally challenging environmental conditions, affects their performance[7-9]. Regardless of the chemistry of the PSAs, van der Waals interactions will decrease by roughly one order of magnitude when switching the interacting medium from air to water[10]. Therefore, some adhesives employed in wet environments necessitate dry bonding, suggesting challenges associated with contact formation in aqueous environments. Depending on the chemistry of the adhesives, the presence of water can also affect other type of surface interactions (e.g. electrostatics, hydrogen bonding), as well as the bulk rheological properties of a PSA. A better understanding of the role of an aqueous environment over the whole pH range on the bonding and debonding processes of PSAs has practical implications in the field of medical adhesives[11], wearable electronics[12], and even transportation[13].

Acrylic-based PSAs are one of the most common class of PSAs, and generally consist of a crosslinked copolymer where the comonomers are selected to control the glass transition temperature (T_g) and the degree of entanglement[14-15]. A common, well-characterized, formulation is that of poly(2-ethylhexyl acrylate), (poly-2EHA) copolymerized with a low weight fraction of acrylic acid (AA), and then crosslinked to obtain poly(2-ethylhexyl acrylate-co-acrylic acid)[16]. Poly-2EHA has a low T_g, and co-polymerization with acrylic acid (high T_g) increases the cohesive strength and introduces polar groups at the surface for better interfacial bonding[17]. In our recent investigation[18], we characterized the change in bonding energy between poly(2-ethylhexyl acrylate-co-acrylic acid) and glass of different functionality in deionized water. During the

bonding process with either a hydrophobic or hydrophilic glass probe, we observed heterogeneous contact formation as well as the presence of large pockets of trapped water (diameter on the order of microns) within the contact region during the early stages of dwell. In the contact region, water can remain trapped at the nanoscale, due to favorable interactions between the water molecules and the opposing surfaces[19]. Macroscale trapped water can also be present because of surface roughness, or maybe due to deformation caused by hydrodynamic drainage occurring during contact formation[20-21]. In fact, we observed that contact formation in water had a more pronounced effect on adhesion when the probe was hydrophilic, where debonding occurred through external crack propagation, than when the probe was hydrophobic and debonding occurred via fingering and cavitation. Independent rheological measurements did not indicate changes in the bulk properties of the PSA caused by water exposure, therefore most of the changes in adhesion could be attributed to changes in the surface properties of the interacting surfaces in water.

The presence of acrylic acid as a comonomer in a PSA should play an important role in modulating the underwater adhesion and should make the performance of the adhesive pH-sensitive. Below the pKa, acrylic acid is protonated and can form hydrogen bonds with a surface. Above the pKa the deprotonated acrylic acid is charged, which can limit hydrogen bond formation, and can lead to repulsive interactions (and a decrease in adhesion). Understanding the role of pH on underwater adhesion of PSAs is also important for medical applications due to the need to maintain a strong bond over a broad range of environmental conditions. For example, transepidermal water loss leads to skin surface pH 4-5[22], sweat has pH between 5-7[23], saliva has a pH 6.5-7.5[24], pH in the colon can reach up to 9[25], and soapy water is usually alkaline with a pH10-12[26]. In addition, dry skin is generally hydrophobic[27], so a better understanding of the role of AA on the bonding and debonding to a hydrophobic surface exposed to different level of acidity is particularly needed. Unfortunately, there is no systematic investigation of the effect of pH on the underwater adhesion of PSAs, especially of PSA containing pH-responsive functionality such as acrylic acid.

Although the role of the acrylic acid comonomer on the underwater adhesion of PSAs has not been investigated, prior studies provide useful insight on the role played by acrylic acid at a polymer surface on adhesion in humid environment. Schindler *et. al.*[28] found that an increase in relative humidity affected the near surface composition profile of polar methyl methacrylate groups in poly(ethylhexyl acrylate-co-methyl methacrylate) with 20% of methyl methacrylate

groups. They also observed a transition in the failure mechanism from fingering instabilities to external crack propagation as the humidity increased. Roy *et. al.*[29] observed that the presence of acrylic acid alters the nature of molecular interactions at the surface, thereby changing the orientation of butyl acrylate in poly(butyl acrylate-co-acrylic acid) as water evaporates from a PSA synthesized in a water emulsion. In addition, PSA from waterborne latex emulsions cast at different pH of the aqueous phase have a lower adhesion when the casting solution pH is higher[7]. In the case of waterborne PSA, the pH of the aqueous solution during the preparation of the PSA affects both the mechanical and surface properties of the polymer film formed after casting[8]. It has been suggested that high pH induces dipolar interactions between deprotonated AA groups and Na^+ cations creating a physical ionomeric crosslinking in the PSA film that could cause the surface to stiffen thereby increasing adhesion. Stiffening of the surface could affect both bond making and bond stability under water. Beyond PSAs, it is well-established that deprotonation of carboxylic acid groups in aqueous solution at high pH leads to higher electrostatic repulsion during approach and weaker adhesion between carboxylic acid and negatively charged silica surfaces[10, 30-32].In contrast to work with SAMs, for acrylic PSAs such as in poly (2-ethylhexyl acrylate-co-acrylic acid), the pKa, mobility, and the segregation to the surface of the AA groups will be affected by their covalent attachment to a polar comonomer, which in turn will modulate the effect of pH on adhesion. Understanding the bonding and debonding mechanisms of acrylate PSAs in aqueous environments of different pHs is needed. In particular, the role played by the acrylic acid comonomer on underwater adhesion is poorly understood.

Here, we investigate the role of acrylic acid groups on contact formation and adhesion of an acrylic PSA to a hydrophobic probe in aqueous environment over a wide range of solution pH. In particular, we aim to quantify how the acrylic acid comonomer impacts underwater adhesion between pH3 and pH11. We also aim to determine the role of solution conditions on the bulk and surface properties of the PSAs to decouple their separate contributions on adhesion at different pHs. To answer these questions, we perform underwater probe tack measurements while monitoring contact formation and debonding using optical microscopy. We also independently characterize the surface properties of the PSAs using contact angle measurements and *in situ* zeta potential measurements. Lastly, we characterize the bulk properties of the PSA (in air and in water) through rheological measurements.

2. MATERIALS AND METHODS

2.1 Materials and sample preparation

PSA synthesis.

Model pressure sensitive adhesives based on copolymers of 2-ethylhexyl acrylate (2-EHA) and acrylic acid (AA) or homopolymers of 2-ethylhexyl acrylate (2-EHA) are synthesized by free-radical solution polymerization. The monomers are mixed with ethyl acetate, as reaction solvent, at a concentration of 30 wt%. 2,2'-Azodi(2-methylbutyronitrile (Vazo 67® from DuPont) is added as thermal radical initiator, at a concentration of 0.05 mol% in amber, narrow necked pint bottles at room temperature to both copolymers and homopolymers. The bottles are located in a water bath at 60°C for 24 hours. The same benzophenone derivative is added as photocrosslinking agent at a concentration of 0.18 mol% to all polymers to obtain equivalent levels of crosslinking. The solutions are deaerated by purging with nitrogen gas for 10 min and capped tightly before starting the polymerization. After polymerization, bottles are cooled to room temperature and the polymer solutions are used for pressure sensitive adhesives. Details of copolymerization and homopolymerization of these model systems can be found elsewhere[18, 33] . PSA samples are then analyzed by conventional GPC against polystyrene molecular weight standards using THF as the solvent and eluent. A sample with a composition of 88 mol% of 2-Ethylhexyl acrylate and 12 mol% of Acrylic Acid having a weight average molecular weight (Mw) of 1,200 kg/mol was selected for the totality of the results showed in this work. A sample of 100 mol% of 2-Ethylhexyl acrylate having a weight average molecular weight (Mw) of 1,200 kg/mol was used as control. These samples were selected based on their similarity in molecular weights (Mw) before crosslinking as well as their equivalence in gel content after UV-curing. Table 1 summarizes detailed GPC characterization of the PSAs as well as gel contents of the final tapes after curing.

All PSA solutions are then knife coated on the same release liner (3M™ Silicone Release liner 5002, 50.8 μm, polyester), dried in a convection oven at an average temperature of 66°C, followed by exposure to UV at a set total adsorbed dose of UV-B light = 400 mJ/cm^2 (directly measured using a power puck radiometer) using a processor from Fusion UV-systems for crosslinking, and used as transfer tapes for further evaluation. Knife gaps were adjusted to obtain thicknesses of 25 μm and 38 μm for copolymer (acid-containing) and homopolymer (control), respectively. Thickness of the homopolymer film was chosen to be higher than that of the copolymer film so

the initial debonding forces from polar surfaces (i.e glass and stainless steel) based on peel values, are in the same order of magnitude and debond cleanly from polar substrates. For rheology measurements, stacks of the same material are used. The gel content was determined as described in the ASTM International standard, D3616-95. A 0.5 g test specimen was placed in a mesh pouch measuring 3.8 cm x 3.8 cm. The specimen was placed in a mesh basket measuring 3.8 cm x 3.8 cm. The basket with the specimen was weighed to the nearest 0.1 mg and placed in a capped jar containing sufficient toluene to cover the sample. The pouch with the specimen was weighed to the nearest 0.1 mg and placed in a capped jar containing sufficient toluene to cover the sample and put on a roller. After 24 hours the basket (containing the specimen) was removed, drained and placed in an oven at 120°C for 30 minutes. The gel content was determined by calculating weight % of the remaining, unextracted polymer to the original polymer sample. Values are reported as the average of three replicas. Standard deviation is typically < 5% within replicas.

Table 1. Composition and molecular weight result of selected PSAs. Results are averages from duplicate injections. M_n = Number-average molecular weight, M_w = Weight-average molecular weight, M_p = Molecular weight at signal peak, $Đ$ = Dispersity = M_w/M_n (Previously known as polydispersity index)

PSA	***Composition***		***M_n***	***M_w***	***M_p***	***Đ***	***Gel Content***
	2-EHA wt% (mol%)	AA wt% (mol%)	kg/mol	kg/mol	kg/mol		wt%
5%AA	95 (88)	5 (12)	287	1199	1175	4	92
0%AA	100 (100)	0 (0)	104	1200	1100	11.6	89

Buffer solutions preparation

One phosphate buffer solution (PBS) tablet (Sigma Aldrich) was dissolved in 500mL deionized water to get a PBS solution with 4mM phosphate buffer, 1mM potassium chloride, and 55mM sodium chloride. Deionized water (>18.2 MΩ•cm) was obtained from EMD Milli-Q® Integral Water Purification System. To generate the buffer solution, 10ml of the 4mM stock solution was diluted in 400 ml deionized water to obtain 0.1 mM phosphate buffer solution. NaOH solution (~pH13) and HCl solution (~pH1) were added into this 0.1 mM buffer solution to adjust pH from

3 to 12. The pH of all solutions was monitored with a Mettler Toledo MP220 pH meter. All pH buffer solutions were stored in a sealed bag filled with nitrogen and stored at room temperature. pH of the buffer solutions was measured again prior to any measurement.

Glass probes. Plano-convex lenses with a radius of curvature 7.06 mm (Edmund Optics) were used for probe tack measurements. These lenses are functionalized with octadecyltrichlorosilane (OTS, Gelest) through solution deposition in toluene after cleaning in oxygen plasma for 5 seconds at 50W. During the OTS deposition, the lenses were placed in a cleaned enclosed glass beaker in a solution containing 80 mL toluene and 160 μL OTS for 20 minutes or 3 hours (until the desired wetting properties were achieved). The lenses are then rinsed with toluene to remove excess OTS and dried at 60°C for 1 hour. The static contact angle of deionized water and hexadecane on OTS coated glass slide were respectively 108±3° and 31±2°.

2.2 Probe Tack measurements.

Experimental protocol. A custom-built normal and lateral multifunctional force microscope (MFM)[34] is used for probe tack measurements. For the measurements, an OTS coated spherical (plano-convex) lens is mounted on the lens holder attached to the cantilever of the instrument. Fiber optic reflection is used to measure the spring deflection, and is calibrated before each experiment. The PSA films are cut into 15 mm x 15 mm sized samples. After cutting, the PET release liner is removed, and a sample is placed gently onto a cleaned and dry 46 x 27 mm glass slide (Ted Pella). A weighted roller (2 kg) is then rolled 20 times onto the sample to remove any trapped air bubbles from the PSA-glass slide interface and apply a high contact pressure. The PSA sample is then mounted on the MFM and held in place by screwing a rectangular holder on top of the PSA-coated glass slide. During a probe tack measurement, the cantilever is lowered at a velocity of 50 μm/s until it applies a 10 mN normal force to the sample, and is held at 10mN using a force feedback loop for a dwell time of 100 s. Subsequently the cantilever is retracted at 50 μm/s. Typical approach, dwell, and detachment traces are given in Supporting information figure S1(b). Throughout approach, dwell, and debonding images are captured at 70 frames per seconds with an inverted microscope with a 5x objective. The procedure for probe-tack tests in air and in aqueous solutions are identical, except that for measurements in aqueous solutions the solution is placed on the sample and contained in the MFM bath 10 minutes prior to contact formation. The measurements are performed at room temperature (approximately 23 °C) and at less than 50% relative humidity. More

details on the parameters and experimental setup are given in our previous work.[18] Each measurement is repeated three times and the reported values represent the average and standard deviation.

Image analysis. Probe tack contact images are processed using ImageJ software (National Institutes of Health, NIH). To process the images during dwell, the out of contact background image is first subtracted from the contact images in aqueous solution, followed by a thresholding and noise reduction steps to improve visualization of the contact area. Subsequently, the images are converted into binary and analyzed through MATLAB to quantify the contact area by calculating the number of black pixels and scaling it by area to number of pixel ratio to find actual image area.

2.3 Rheology

Rheological measurements were performed on the two PSAs investigated on an AR1500ex rheometer (TA Instruments) using an 8 mm diameter parallel plate geometry as the measuring system. The samples were prepared by soaking 4 cm x 4 cm strips cut out from sheets of PSA in the desired pH solution for ~10 minutes. The sample was then folded together to create an 8 mm diameter layered mass and loaded in the gap which was set at 2.2 mm. Amplitude sweep experiments were also carried out at an angular frequency of 1 rad/s to ensure that the samples were being probed in the linear viscoelastic regime. A strain amplitude of 1% was used in frequency sweep experiments (1-100 rad/s) to obtain the storage (G') and loss (G'') moduli of the PSAs. The measurements were carried out while the sample was submerged in the desired pH solution using an immersion cup. The duration of each measurement was ~3 minutes. All the measurements were carried out at 22.4 °C. Each measurement is repeated three times and the reported values represent the average and standard deviation.

The rheology of polymers also gives insight into their relaxation timescales and mechanical properties. Crossover frequency (ω_c) is the frequency at which the loss modulus becomes larger than the storage modulus. The terminal relaxation time ($\tau_c = 2\pi/\omega_c$) can be calculated from the crossover frequency and is less than 0.06 s for 5% AA and is even lower for 0%AA PSA. Therefore, a dwell time of 100 s during probe tack measurements is much higher than this relaxation time, and gives the PSAs sufficient time to relax prior to debonding.

2.4 Contact angle measurement

Contact angles of fluids drop on PSA sample were measured by a goniometer (FTA 125, First Ten Angstroms). A 10 µL sessile droplet is placed on the surface of the PSAs. Advancing and receding contact angles are measured by injecting or retracting fluid from the deposited sessile droplet by syringe pump via a glass capillary needle. The flow rate of fluids is fixed at 20 µL/min. Advancing contact angle is measured first, followed by the receding contact angle. Capillary needle, glass syringe, and plastic tubings are kept in RBS cleaning solution for 24 hours. They are rinsed with deionized water, dried with nitrogen. rinsed with the probe fluid and filled with the probe fluid prior to use. Every data point is repeated at least 3 and average values are reported along with the standard deviation.

The fluids used in contact angle measurement are buffer solutions of different pH as well as diiodomethane (Alfa Aesar). Diiodomethane is kept in the dark to slow down its decomposition upon exposure to light. The surface tension of the fluids is measured from a pendant drop in air. The reported value[35] of deionized water is 72.8 mJ/m^2. For pH buffer solution, the effect of pH on surface tension is not significant and we obtain 73 $\pm$ 1 mJ/m^2, in agreement with literature reports[35]. The measured average surface tension[36] of diiodomethane is 47 $\pm$ 1 mJ/m^2 while reported value[37] is 50.8 mJ/m^2. In water, the surface tension of diiodomethane decreased to 39 $\pm$ 1 mJ/m^2. Based on Fowkes' method[36], the dispersion and polar surface tension of diiodomethane we used was calculated to be 45 $\pm$ 1 mJ/m^2 and 2 $\pm$ 1 mJ/m^2, respectively. All following calculation involving the surface tension of diiodomethane uses these measured values.

2.5 Surface Zeta Potential measurements

PSA samples were cut into small 7 mm x 4 mm strips and attached to the sample holder for the measurement of surface zeta potential (SZP, i.e. the zeta potential of the PSA-aqueous surface) using Malvern Zetasizer NanoZS surface zeta potential accessory (ZEN1020 Sulfate functionalized polystyrene latex particles (SLPs) of 100nm diameter (Thermo Fisher Scientific) are then dispersed in solutions of different pH. The accessory is immersed in the solutions for SZP measurements. SLPs have a stable negative zeta potential of -20 to -50 mV over pH3-pH11. OTS coated glass sheets were cut into small strips of 7mmx4mm and attached to the sample holder using 3M VHB tape for SZP measurements. The Zetasizer software uses phase analysis light scattering (PALS)[38] to obtain the zeta potential of the tracer particles at different distances from the surface of interest (125, 250, 375 and 500 µm) using the Smoluchowski equation ($U_E = \frac{\varepsilon\zeta}{\eta}$), where the electrophoretic

mobility of the particles U_E is converted into the zeta potential ζ of the particle, and ε is the dielectric constant of the fluid while η is the viscosity of the fluid. The software then fits the apparent tracer zeta potential as a function of distance to a straight line where the intercept is the apparent zeta potential of the particle very close to the surface (see Supporting Information Figure S3). From these measurements, the surface zeta potential ($\zeta_{surface}$) is obtained from the difference between the zeta potential of the particle far from the surface and the zeta potential of the particles close to the surface ($\zeta_{surface} = \zeta_{tracer,true} - \zeta_{tracer,apparent}$). Each measurement is repeated thrice and average value is reported along with the standard deviation.

3 RESULTS AND DISCUSSION

3.1 Effect of acrylic acid during debonding in air

We first investigate the effect of the acrylic acid comonomer on the adhesion and rheology of the PSAs in air (see Figure 1). These measurements can be compared to literature reports[9, 14], and serve as a control and reference point for experiments under water. The two PSAs studied here are poly(2-EHA), which we label as **0%AA** (dashed) and poly(2-EHA-co-AA) containing 5 wt % of acrylic acid, which we label as **5%AA** (see Table 1). When comparing the two PSAs we see that under identical conditions the presence of AA leads to higher debonding forces from a hydrophobic probe (Figure 1a). In addition, we observe that the debonding mechanism for both PSAs in air is fingering at the periphery and sometimes the formation of one or two cavities during debonding. Throughout the mode of failure is always adhesive.

The increase in the debonding force with the addition of AA is consistent with previous work on the effect of acrylic acid comonomer in acrylic PSAs. Poly(acrylic acid) has a higher T_g than poly-(2EHA), and therefore increases the cohesive strength of the polymer. We see that G' and G'' are larger for 5%AA than for 0%AA at all frequencies, including 8-13 rad/s which is close to the estimated strain rate during debonding (motor velocity/PSA film thickness). As a result of its higher elastic and storage moduli, the 5% AA PSA can both store and dissipate more energy than the 0% AA PSA, leading to higher adhesion.

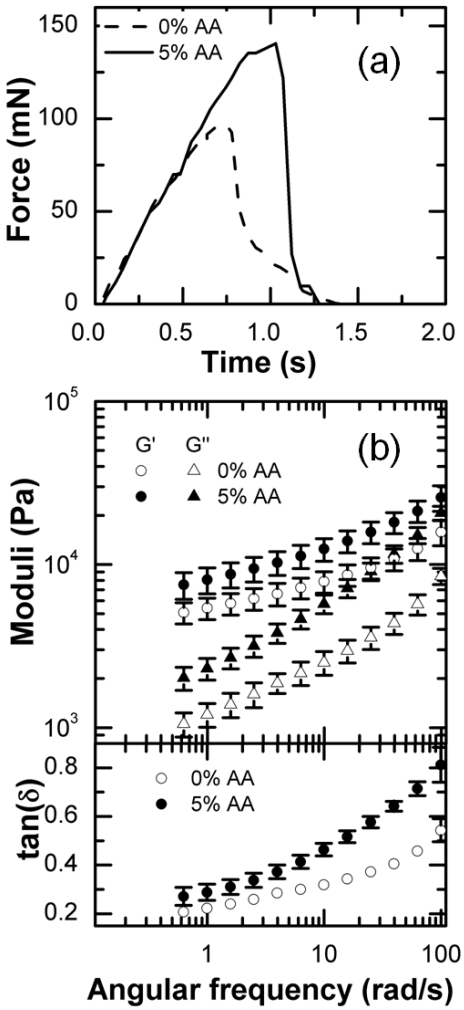

Figure 1. (a) Force−time plots during debonding of 0%AA (dashed) and 5%AA (solid) PSAs using an OTS-functionalized glass probe in air. Debonding forces are measured after identical dwell conditions (100 s at 10 mN) and identical retraction rate (50 μm/s). (b) Storage (G') and loss (G'') moduli and (c) tanδ as a function of angular frequency for 0%AA (open) and 5%AA (fill) in air. Error bars have been removed when they are smaller than the markers.

3.2 Role of AA on underwater contact formation and debonding

We perform debonding measurements in aqueous solution of pH3-pH11(Figure 2a,b) for the two PSAs under investigation. Note that we introduce water prior to contact formation. As shown in Figure 2a, we do not observe a significant effect of the environment (air, pH) on the debonding of the PSA without AA (0%AA). Similarly, in the absence of AA in the PSA both the storage modulus (G') and the loss modulus (G'') are unaffected by the environmental conditions. (Figure 2c).

In contrast, incorporating 5% AA to the PSA leads to debonding forces that are very sensitive to their environment (Figure 2b). First, we see that at pH3, the maximum force of debonding is comparable to that in air. Then, as the pH increases, the maximum debonding force decreases and is lower than the one measured in air. In fact, at pH11 the debonding curve for the two PSAs are nearly identical. Moreover, in contrast to 0%AA, we do observe a slight decrease in both G' and G'' when the environment is switched from air to water. Note that as the rheological properties are measured over the full thickness of the polymer. We cannot rule out local plasticization of 5%AA, however water absorption and thereby swelling is limited due to the small percentage of acrylic acid[39] and short 10-minute immersion in buffer solutions. In our earlier work we did not observe a meaningful change in the rheological properties for samples immersed for up to 4 hours in DI water.[18] Moreover, once in an aqueous environment, the rheological properties of 5%AA are not affected by the solution's pH. Hydrogen bonding between carboxyl-hydroxyl or carboxyl-carbonyl groups within the polymer network could be disrupted at higher pH, however if it occurs it does not appear to affect the bulk mechanical properties possibly due to limited water absorption. Therefore, the rheological measurements of 5%AA suggest that the pH dependence of adhesion is more due to a change in the surface than of the bulk properties of the PSA.

For all measurements, the slope of the force-displacement curve in the linear regime prior to the peak force is caused by the system's compliance (PSA and cantilever). Detailed information showing the relationship between the slope and the compliance of the system is given in Supporting Information section 1.2. Beyond the peak force, at pH11 0%AA has a broader force curve (detachment occurs over a longer period of time) than 5%AA. We see that at pH 8 and pH 11 the peak forces are still larger but much closer to the one measured for 0%AA. As a reference in air the addition of AA as a comonomer leads to a peak debonding force that is 1.4 times larger. In summary, for underwater and air measurements, the addition of 5 wt% of acrylic acid comonomer to poly-(2EHA) increases the maximum debonding force, except at pH11. For measurements at pH11 the maximum debonding forces for the two PSAs are comparable.

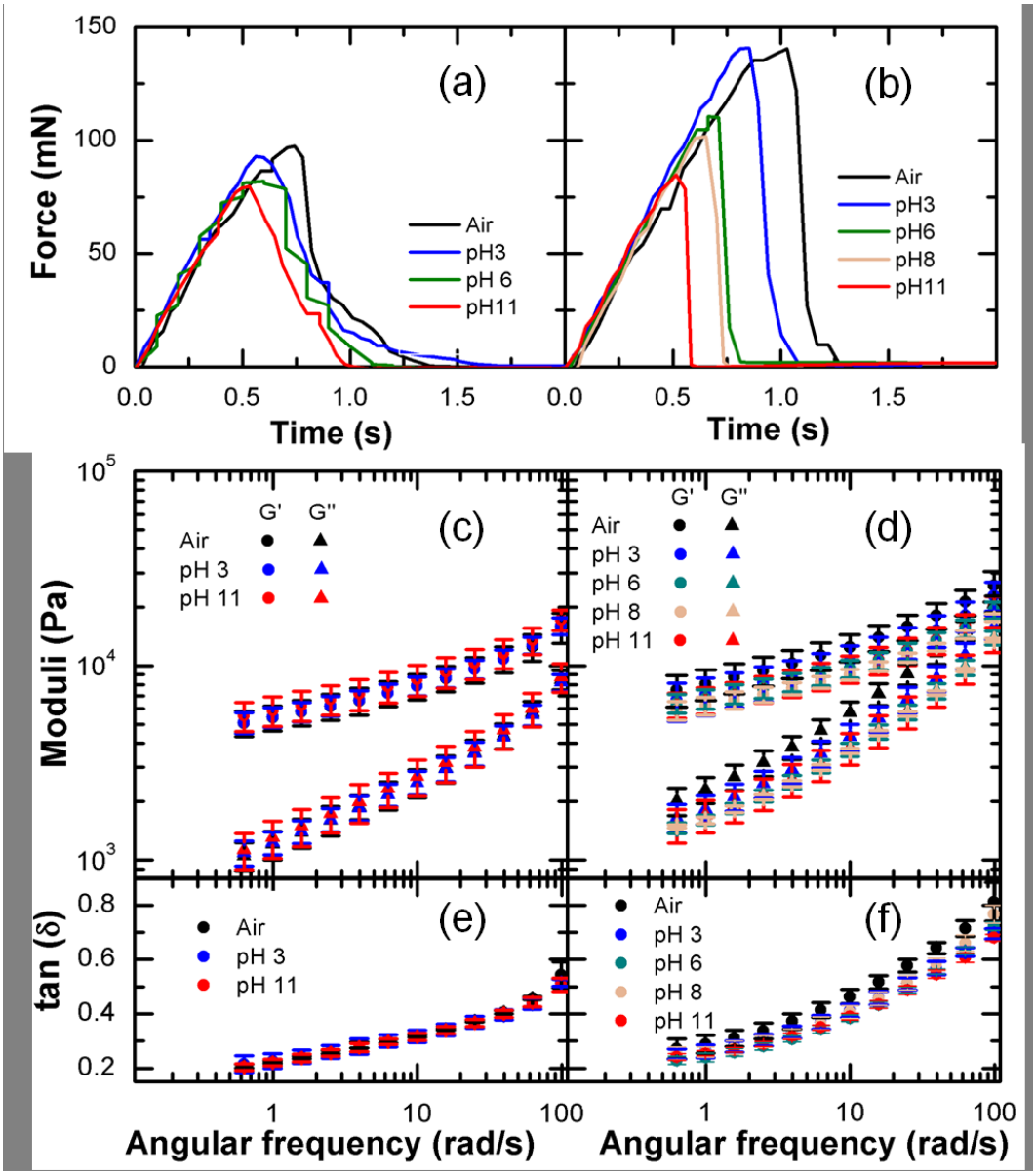

Figure 2. Force−time plots for 0%AA (a) and 5%AA (b) during debonding with OTS functionalized glass probe in aqueous solutions of different pH and and compared to the same measurements in air. Debonding forces are measured after identical dwell conditions (100 s at 10 mN) and identical retraction rate (50 μm/s) in the same medium as for debonding. Storage, loss moduli and tanδ as a function of angular frequency for 0%AA (c,e) and for 5%AA (d,f) PSAs.

We also monitor the initial contact formation and relaxation using optical microscopy (Figure 3). We only show the contact formation for 5%AA PSA but did measure the maximum contact area for 0%AA (prior to debonding) and observe similar heterogeneous contact formation as those observed with 5%AA and shown in Figure 3. We find that the maximum contact area

(after dwell) for the 0%AA is usually 1.5 times larger than for the 5%AA PSA. In addition, we observe that for both PSAs the contact formation and growth in air is homogeneous (within the resolution limit of optical microscopy), while it is heterogeneous in all aqueous solutions. In our prior work we also observed similar heterogeneous contact formation with hydrophilic and hydrophobic probes during the initial stage of dwell for bonding in DI water[18]. Here we show that the contact regions are not only heterogeneous but also appear sparser during the initial stage of dwell as the pH increases. We can quantify the growth of the contact area as a function of time for 5%AA PSA (Figure 3b). We see that the dwell time of 100s gives the PSA sufficient time to relax, as the contact area increases by less than 5% from 10s to 100s. We quantify the difference in contact formation and growth between measurements at pH3 and those taken at pH11. Most of the effect of pH on contact formation occur before the set point in dwell force is reached, and over a timescale that is of order of the terminal relaxation time (approximately 0.06s here). Our analysis shows that initially the contact area formed between the probe and the PSA at pH3 is larger than at pH11. We also find that the contact area grows faster initially if the surrounding solution is at pH3 than at pH11. Therefore, contact between the PSA and the probe is more favorable at pH3 than at pH11. At higher pH the AA groups are more likely to be deprotonated and bear a negative charge. The negative surface charge density could lead to electrostatic repulsion between the probe and the substrate. More discussion of the possible role of electrostatic interactions is present in the next section. Note that, within the resolution of optical microscopy, we do not observe air trapped on the surface during contact formation. Nanobubbles smaller than our detection limit could also be present on the surface, as we are making contact between two hydrophobic surfaces in water[40-41]. However, we do not see multiple cavitation sites during detachment as observed by Davis *et. al.*[42], likely due to the long dwell time (when compared to the polymer relaxation time) in our measurements.

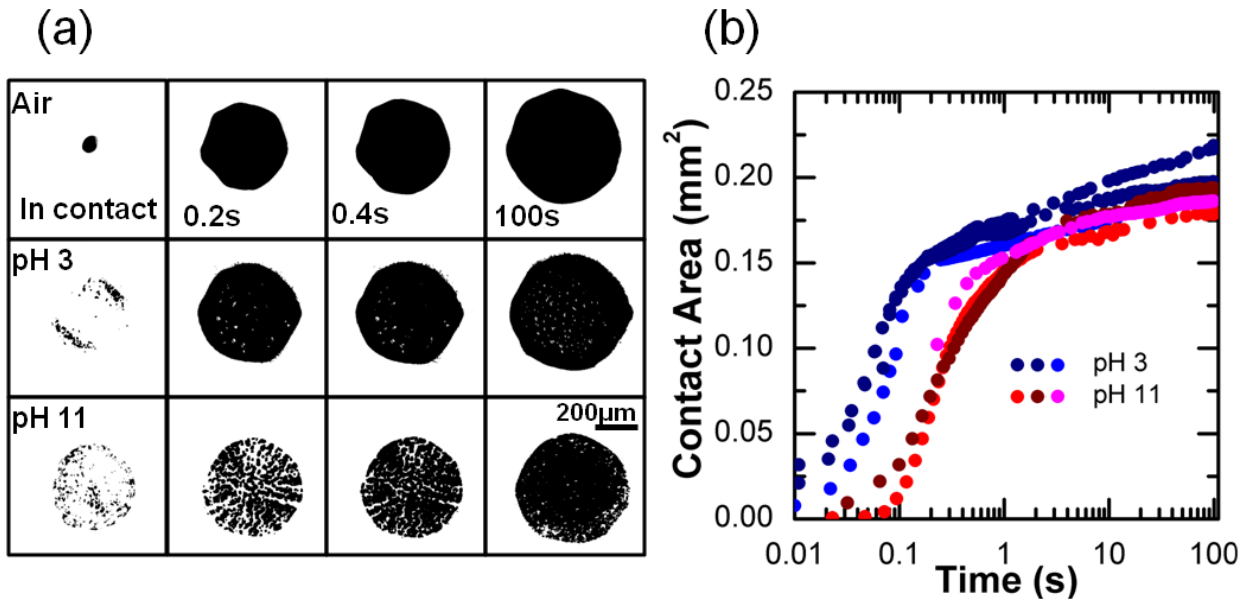

Figure 3. Contact images (a) and contact area (b) during contact formation and growth during the dwell time prior to debonding measurements for 5%AA. The applied force during dwell is 10.0 mN ± 1.4 and controlled using a feedback loop. For the feedback loop the setpoint is reached within 1s. Shades of red are three replicates for pH11 whereas shades of blue are three replicates for pH3 in (b).

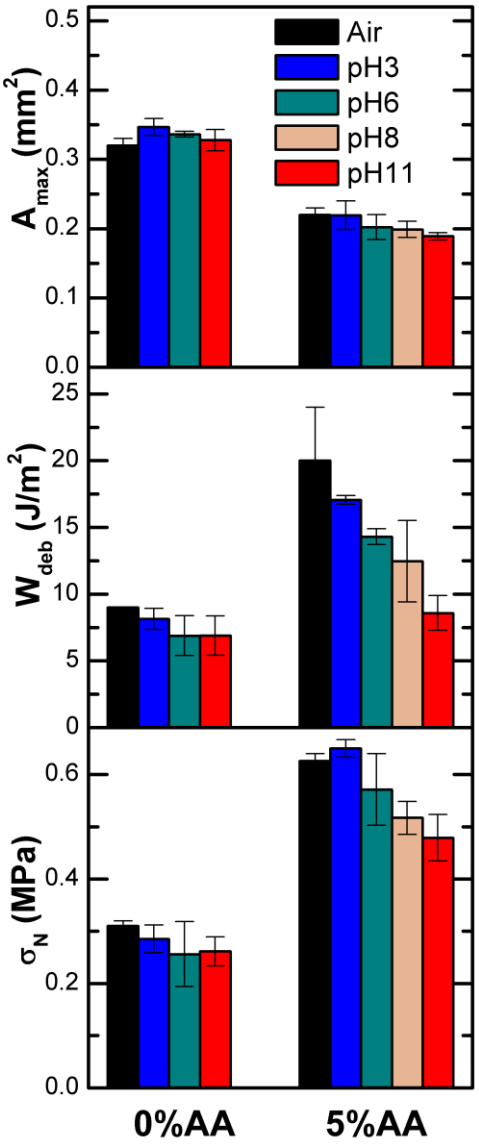

Figure 4: (a) Maximum area before detachment (A_{max}), (b) Work of debonding (W_{deb}) and (c) nominal stress (σ_N) for 0% AA PSA and 5% AA PSA debonding from OTS functionalized glass probe in different environments.

Comparing only the maximum force of debonding is insufficient to understand the role played by the AA on adhesion, as contact area before debonding can also vary and plays an important role in the adhesion of PSAs. Therefore, we image contact formation using optical microscopy and evaluate the maximum projected area of contact between the PSA and the glass probe (obtained at the end of the dwell period). Calculating the real contact area in the shape of a spherical cap by considering the curvature of the probe leads to a contact area that is 0.06% larger

than the projected area. In general, we see that 0%AA has larger contact area than 5%AA (Figure 4a). The lower elastic modulus of 0%AA PSA makes it more compliant, and the PSA can deform more readily during dwell for the same normal force. The effect of elastic modulus on the contact area has been shown in more detail in a previous study[43].

A higher contact area can increase the maximum force of debonding due to an increase in area for surface interactions, but also due to a larger interface to dissipate energy. Therefore, we also characterize the effect of AA on the nominal stress (σ_N) and work of debonding (W_{deb}), both quantities are normalized by the maximum contact area. Nominal stress is the maximum force of debonding divided by the maximum contact area. The work of debonding is calculated by integrating the area under force-displacement curve and normalizing it with the maximum contact area before detachment. As we have shown in Figure 1a, the maximum debonding force in air is lower for 0%AA than for 5%AA. Thus, a larger contact area for 0% AA implies even lower nominal stress and work of debonding in air as compared to 5% AA (Figure 4b-c) as observed.

For both PSAs we find that a change in pH had little effects on the maximum contact area, and thus the variation in nominal stress or work of debonding is similar to that of the peak debonding force. Looking at the maximum contact area for 0%AA in air and in different pH solutions, we only see small variations that are in the range of the standard deviation. Thus, insignificant changes in maximum contact area are observed for 0%AA in air and pH solutions. These observations are consistent with rheological measurements where we showed that the presence of an aqueous solution had no effect on rheological properties or adhesion of 0%AA PSA (Figure 2c). The same observations stand for the work of debonding and nominal stress, which remained unchanged in aqueous solution.

For 5%AA, we observe similar nominal stress in air and at pH3, but higher work of debonding in air than at pH3 (broader force curve in air). Increasing the pH leads to a significant decrease of the work of debonding and nominal stress, while there is only a minimal decrease in the contact area with pH (Figure 4). More specifically, the work of debonding decreases by a factor of two as the pH increases from pH3 to pH11. Looking back at the rheological properties of 5%AA shown in Figure 2d, we see negligible effect of pH on both storage and loss moduli. Hence, bulk rheology cannot account for this change in work of debonding at different pH for 5%AA. We

would expect the addition of acrylic acid groups to affect the surface properties of the PSA at different pH which could lead to a variation in adhesion at different pH.

3.3 Surface zeta potential

We measured the surface zeta potential (SZP, ζ) of the PSAs as well as that of OTS coated glass slides in pH buffer solutions using tracer particles (Figure 5). An outline of this method is provided in section 2.5 with more details in the Supporting Information Section 4. We observe that the SZP of 0%AA is nearly constant at -48 mV and shows little to no variation with pH. The SZP of the OTS probe also does not change much with pH, although it shows some variation from –15 ± 6 mV at pH3 to -52 ± 7 mV at pH11. In the absence of carboxylate groups, there is a net negative charge on both the surface of 0%AA and of OTS. Hydroxide ions preferentially adsorb on hydrophobic surfaces (such as OTS and P(2-EHA)) in water leading to a negative surface potential.[44-45] In contrast to 0%AA and OTS, the SZP of the 5%AA is a strong function of pH, ranging from -1 ± 32 mV at pH3 to -100 ± 7 mV at pH11. Based on these measurements the surface charge density estimated by Grahame equation[10] changes from -0.01 $\mu C/cm^2$ at pH3 to -2.1 $\mu C/cm^2$ at pH11. Likely the SZP becoming more negative with an increase in pH is due to deprotonation of the AA comonomer present on the surface leaving negatively charged COO^- groups on the surface. Similar results were reported for the study of polystyrene-polyacrylic acid block co-polymers[46]. Interestingly, a linear relationship between SZP and pH is expected, and can be analytically derived for 1:1 electrolyte[47].

Electrostatic repulsion between two surfaces could impact the bonding process, or contact formation[48]. The initial contact area of 5%AA, estimated using the first image of contact, decreases from 0.011±0.010mm^2 at pH3 to 0.002±0.001mm^2 at pH11. The instantaneous rate of contact formation peaks and is almost thrice at pH3 (1.5mm^2/s) than pH11 (0.5mm^2/s) in the initial stages of contact formation (below 0.1s) after this point the rates of growth in the contact areas are similar and likely determined by the polymer relaxation dynamics (Figure 3b). The effect of solution conditions on the bonding process will be the subject of future investigations, as it is difficult to decouple the effect of electrostatic repulsion and force feedback loop during dwell on the contact area.

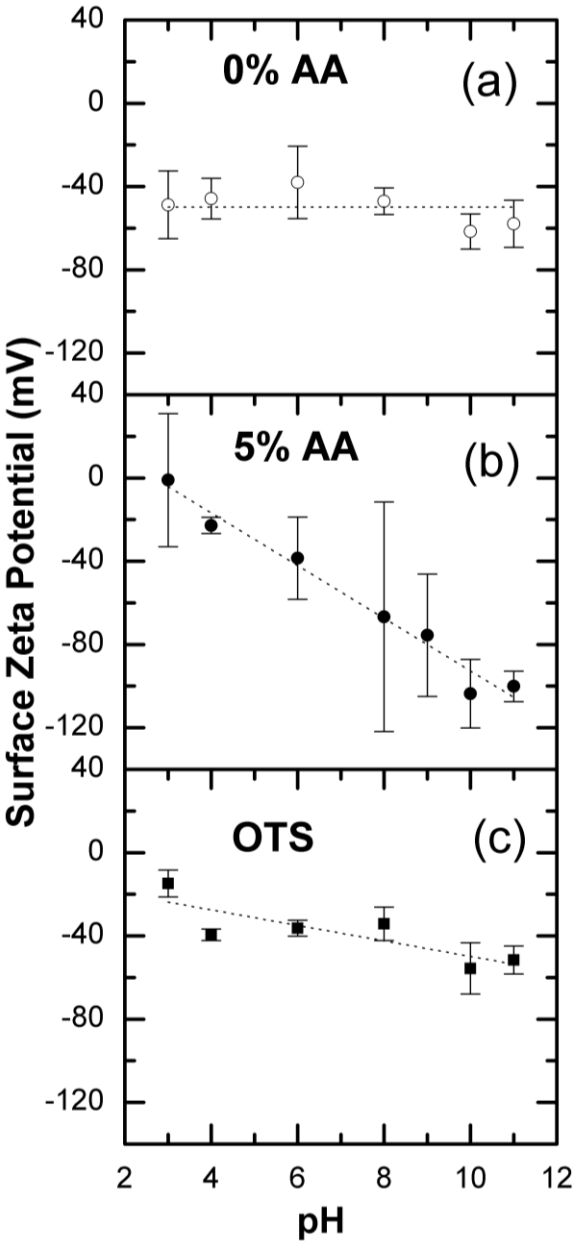

Figure 5. Surface Zeta Potential of (a) 5% AA PSA (b) 0% AA PSA and (c) OTS probe at different pH. Dotted lines are to guide the eye.

3.4 Wetting properties of the PSAs

3.4.1. Contact angle hysteresis of the PSAs. The advancing and receding water contact angles of the pH buffer solutions on both PSAs are shown in Table S2 in supplementary information. The water advancing contact angle on both PSAs is around $\theta_{adv} = 124^{o}$ at all pH. The receding contact

angle on 0%AA is constant across different pH around $\theta_{rec} = 62^o$. A large contact angle hysteresis of $\theta_{adv} - \theta_{rec} \approx 60^o$ is observed for both PSAs. We only observe a pH dependence on the receding contact angle of the 5%AA samples, where the receding angle decreases from $\theta_{rec} = 62^o$ to $\theta_{rec} = 47^o$ when the pH increases from pH3 to pH11. In the absence of AA groups (0%AA), the surface is not pH responsive and there is no sensitivity of the contact angle to the pH of the probe fluid (advancing and receding). When the contact line of a buffer droplet advances it makes contact with a surface that was initially dry and unaffected by the pH. In contrast, when the contact line recedes it moves on a surface that was in contact with the buffer solution, which can explain why the receding contact angle varies with pH but not the advancing angle. For the receding angle on 5%AA we see a plateau region at 3<pH< 6, and a sharp decrease in the contact angles in the region 6 < pH <12. We suspect that acrylic acid groups on the surface of 5%AA will deprotonate as the pH increases and affect contact angle measurements. Note that the roughness of PSAs sample also plays an important role on the contact angle hysteresis. Even in the absence of carboxyl groups, 0%AA still has a large contact angle hysteresis (that is not pH dependent). Finally, rheology measurements show that the elastic modulus of the PSAs sample is around 10-100 kPa, which means that elastocapillarity effects could alter the contact angle measurements and their interpretation.[49-50] Fortunately, for a macroscopic droplet (mm), this phenomenon has a very limited effect on contact angle measurements, even for surfaces as soft as the PSAs investigated here.

3.4.2. Contact angle titration of the 5% AA PSA

Based on the pH dependence of the receding angles on 5%AA, we perform a pH titration analysis to calculate the apparent pK_a of the PSA, as shown in Figure 6. We hypothesize that the acrylic acid group is deprotonated at high pH and protonated at lower pH, a difference that is captured by the receding contact angle measurements. The rapid change in contact angle close to pK_a of surface is expected as cosθ has a sigmoidal relationship with pH (see Supporting Information Section 2.1 for the titration equations and details of the experimental protocol). Using this analysis, we obtain an apparent pK_a for 5%AA of 8.7 ± 0.2 (Figure 6). The pK_a of monomer acrylic acid is 4.25 at room temperature, which is significantly lower than the apparent pK_a of acrylic acid in co-polymerized in p(2-EHA). However, several studies have observed an apparent pK_a ~8 of carboxylic acid SAMs in aqueous solution[30, 51-52]. Due to dissociation of the surface

carboxylic acid groups, the pH at the surface of PSA would be lower than the bulk pH[52]. The real proton concentration near the surface is higher than the bulk and can be approximated as a Boltzmann's distribution, which means that the true pK_a of the PSA is likely lower than the apparent pK_a. Furthermore, pK_a of acrylic acid groups has been shown to increase in presence of surrounding hydrophobic groups[53-55]

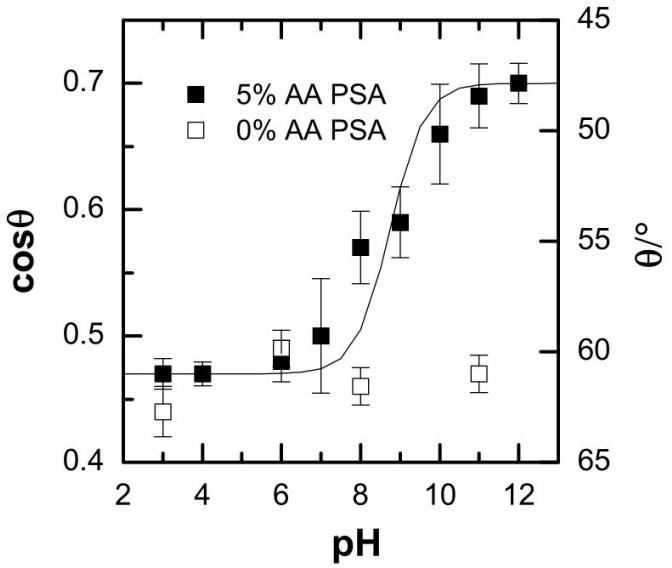

Figure 6. Receding contact angle of pH buffer drops measured on 5%AA (filled) and 0%AA (open). Solid line is the pH titration curve based on the receding contact angle on 5%AA. Detail of the calculations for the pK_a are given in supporting information section 2.1.

3.4.3. Determination of the PSAs-water surface energy. We use the method developed by Fowkes, Owens, et al[56] (detailed in Supporting Information section 2.2) to estimate the surface energy of the two PSAs investigated, as shown in Figure 7. This method assumes that the interfacial energy can be divided into independent and additive polar and dispersion components[57]. We use two probe fluids: pH buffer solutions and diiodomethane to evaluate the surface energy of the PSAs as a function of pH. The contact angles of diiodomethane on both 5%AA and 0%AA are nearly identical. To find the PSA-water surface energy we select the receding contact angles because they capture the PSA after it has equilibrated with an aqueous solution (values reported in Supporting Information Table S3).We find that the surface energy of 0%AA is independent on the solution pH. For 5%AA, we observe that (1) the dispersion component ($\gamma_1^{Rec,d}$) is approximately independent of pH while the polar component (

$\gamma_1^{Rec,p}$) increases with pH; (2) For pH < 6, 5%AA and 0%AA have similar surface energy and components; and (3) the PSA-water interfacial energy decreases with increasing pH. The surface energy result also suggests that the dispersion components of the PSAs in water is approximately independent with pH for both 5% AA and 0% AA.

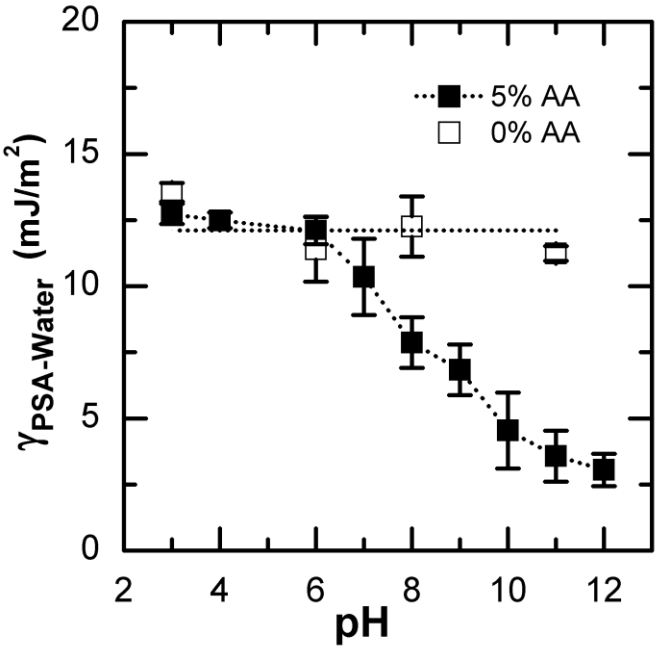

Figure 7. PSA-water surface energy of 5% AA in pH medium (solid square), 0% AA in pH medium (open square) calculated by receding contact angles. Dotted lines are to guide the eye. PSA-air surface energy of 5%AA is 45mJ/m^2 and 0%AA is 46mJ/m^2.

Falsafi *et. al*[58] measured the surface energy in air of a co-polymer with a similar chemistry but higher rigidity using contact mechanics (90% 2-EHA, 5% AA and 5% 1,6-hexanediol diacrylate (1,6-HDDA)). Considering the nearly identical compositions, we would expect the surface energies in air of their PSA and our 5%AA PSA to be similar. Through JKR measurements, they obtain a polymer-air surface energy of 30 mJ/m^2 from bonding and around 60mJ/m^2 from debonding data. Whereas, we obtain 8mJ/m^2 (advancing) and 45 mJ/m^2 (receding) from contact angle measurements using DI water and diiodomethane as fluid probes. When comparing with our measurements, we obtain comparable values of the surface energy in air of 5%AA when we rely on the receding contact angle. The value based on the advancing contact angle measurements likely underestimate the surface energy because of the surface roughness of the PSAs (overestimate the contact angle)[59]. An alternative *in-situ* approach to estimating the change in surface energy of the

PSA-fluid interface based on Saffman-Taylor instability analysis[60] also points to a decrease in surface energy with pH (See Supporting Information Section 6).

3.5 Decoupling of surface and bulk effects of AA on underwater adhesion

We observe a strong correlation between the work of debonding and the surface energy as obtained via contact angle measurements (Figure 8a). For 0%AA we do not observe any significant changes in work of debonding, bulk shear or elastic moduli, surface zeta potential or surface energy of the PSA under the experimental conditions investigated here (~ 10 minutes exposure to solution of varying pH). In contrast, for 5%AA we find that both the surface zeta potential and the surface energy decrease as the pH increases. We also find a strong correlation between the work of debonding and the surface zeta potential (Figure 8b). As the PSA surface becomes more negatively charged (with an increase in pH), we expect stronger repulsive interactions between the negatively charged probe and the PSA. The maximum electrostatic repulsion at pH 10 calculated using 1D Poisson-Boltzmann equation and the measured SZP values is 15 μN, which is higher than the 2 μN predicted at pH4 (see Supporting Information Section 5 for details).

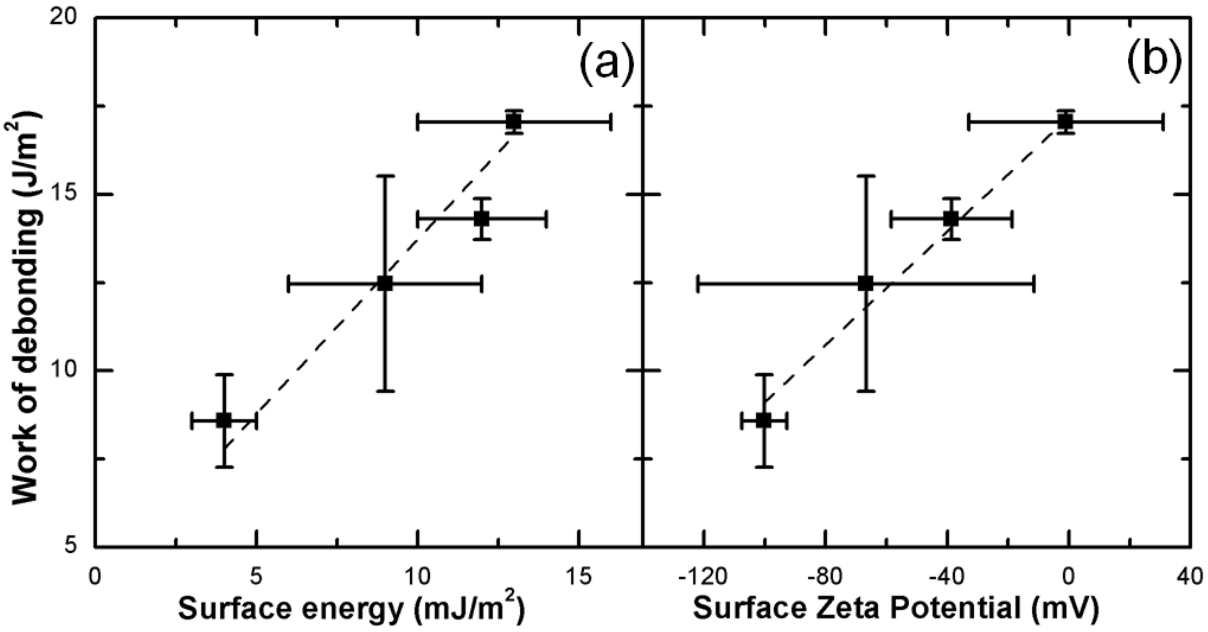

Figure 8: (a) Measured work of debonding (from Figure 4c) versus the surface energy of the PSA-water interface for 5%AA (from Figure 7). (b) Work of debonding (from Figure 4c) versus surface zeta potential of 5% AA (from Figure 5). Dashed lines are to guide the eye.

The effect of the pH of the solution on the surface energy of PSA in water was discussed in the previous section. However, for adhesion with hydrophobic probe, the interaction of PSA with the probe in solution determines the work of adhesion. To approximate the work of adhesion, the surface energy of the probe is also necessary. The thermodynamic work of adhesion of the two PSAs from a hydrophobic probe in aqueous solutions of different pH can be estimated from the receding contact angle measurements[10] using:

$$W_{adh} = \gamma_{13} + \gamma_{23} - \gamma_{12} \tag{1}$$

$$\gamma_{ij} = \left(\sqrt{\gamma_i} - \sqrt{\gamma_j}\right)^2 \tag{2}$$

In equation (1), the subscripts 1, 2 and 3 represent the PSA, OTS probe and medium, respectively. We measure γ_{13} directly, see Figure 7, whereas γ_{23} and γ_{12} are approximated from equation (2), where γ_{ij} represents the interfacial energy between i and j. The surface energy in air for the PSA (γ_1) is evaluated by using receding contact angle measurements of DI water and diiodomethane where we obtain values of the 45mJ/m^2 for 5%AA and of 46mJ/m^2 for 0%AA The surface energy of the OTS surface in air, γ_2= 20 mJ/m^2, is obtained from the literature[61]. We then estimate the work of adhesion in air, from equation (2). For both PSAs the work of adhesion is higher in air (64-65 mJ/m^2) than in pH buffer solutions, as we would expect based on higher dielectric constant of water. For 0%AA we observe a slight decrease in adhesion from 24 mJ/m^2 at pH3 to 21 mJ/m^2 at pH11, which could be possibly due to ion adsorption from the buffer solution onto the hydrophobic PSA surface. For 5%AA we found that the work of adhesion between the probe and the PSA decreases significantly from 23±3 mJ/m^2 f at pH3 to 14±1 mJ/m^2 pH11.

Bulk dissipation increases significantly the work required to debond a PSA beyond the thermodynamic work of adhesion. The separate contributions of surface and bulk dissipation on the work of debonding is typically given using equation (3):

$$W_{deb} = W_{adh}(1 + \Phi) \tag{3}$$

where enhancement of adhesion from the bulk is captured by the dissipation factor Φ.[62] For a soft adhesive attached to a hard substrate the dissipation factor Φ has been used to describe the viscoelastic dissipation in the adhesive.[62] It is a temperature and rate dependent quantity described using various semi-empirical forms[15, 63-64]. Therefore, it is possible to treat Φ as a

quantity that depends purely on the viscoelastic properties of the material and that can be determined from rheological measurements.

We can attempt to extract the value of the dissipation factor Φ for our probe tack experiments to see if it varies with the solution pH. In our probe tack measurements, we have set the debonding velocity to 50μm/s, however the rate of approach of fingers decreases in air as compared to pH solution. We can estimate Φ based on the difference between the work of debonding measured from probe-tack (Figure 4b) and the work of adhesion obtained from contact angle measurements, and shown in Figure 9.

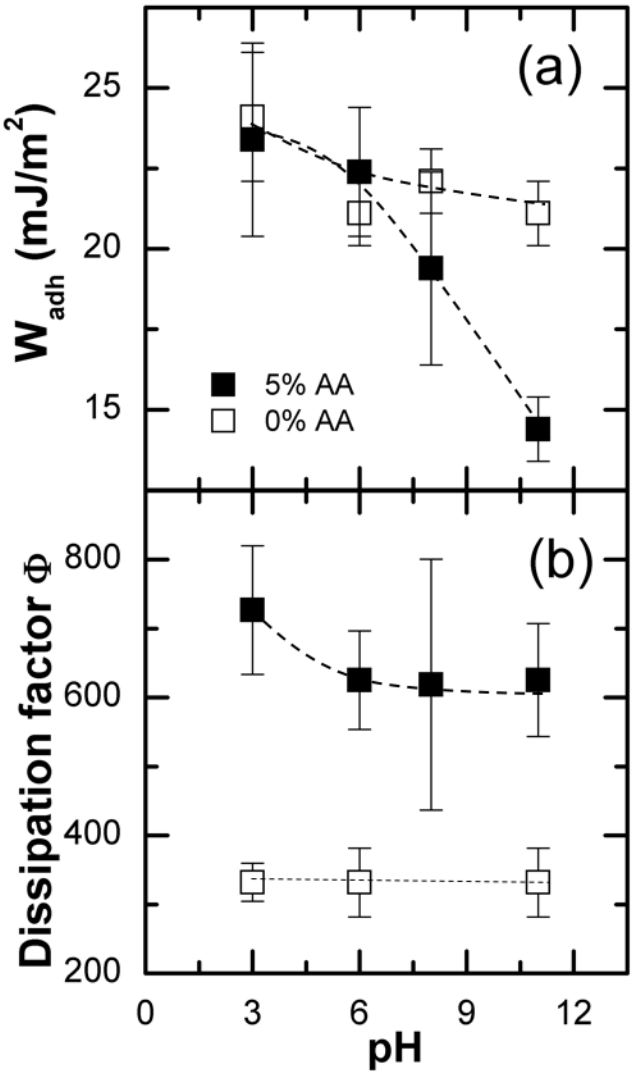

Figure 9: (a) Work of adhesion and (b) Calculated dissipation factor (Φ) for adhesion at different pH for 0% AA (open) and 5% AA PSAs (filled). The work of adhesion in air is 65 mJ/m^2 for 0% AA PSA and 64 mJ/m^2 for 5% AA PSA. Dotted lines are to guide the eye.

We see that changing the environment from air to different buffer solutions influences the value of Φ for both PSAs investigated. For both the PSAs, Φ calculated in air is lower than that in water. For 0% AA, Φ in pH solutions ranges from 332 ± 28 to 332 ± 40 while in air it is 138 ± 46. For 5% AA, it ranges from 619 ± 182 to 727 ± 93, while in air it is 311 ± 62. A semi-empirical functional form[64] of Φ depends on the crack propagation velocity as $(a_T v)^{0.6}$. From calculating the radial velocity of fingers right before the peak force, we find that the radial velocity of the fingers in air ranged from 80-390 μm/s whereas in pH solution it ranged from 200-4400 μm/s for 5% AA PSAs. As the radial velocity of fingers is consistently lower in air, the dissipation would be expected to be lower in air as well, consistent with the previously observed dependence on crack velocity v. There are numerous sources of errors associated with the work of adhesion values calculated, especially when comparing value in air vs values in water. For instance, the contribution of the surface roughness of the PSA on contact angle measurements. Therefore, caution in interpreting the results is necessary, especially when comparing results in air and in water. However, the effect of the solution pH for 5%AA should be less sensitive to the effect of roughness on the receding angle measurements. Acrylic acid is incorporated into PSAs to provide cohesiveness, partly through hydrogen bonding, as well as to increase interactions with the substrates[65]. Reversibility of hydrogen bonds can also lead to increase in energy dissipation[66-67]. The apparent decrease in Φ with the solution pH for 5%AA could indicate that water absorption leads to deprotonation of the AA in the bulk near the PSA-water interface (not only at the surface), therefore disrupting some of the hydrogen bonding and, in turn, decrease the bulk dissipation in the bulk of the PSA as the pH increases.

4 CONCLUSIONS

We investigated the effect of acrylic acid groups on the underwater adhesion of pressure sensitive adhesives at different pH solutions (between pH3 and pH11) at low ionic strength. We observed that the presence of AA as a comonomer leads to pH-responsive adhesion. In particular, we found that the adhesion decreased significantly if the solution pH increases. The maximum nominal stress decreased by 1.4 times and the work of debonding decreased by a factor of 2

between underwater adhesion at pH3 and pH11. In the absence of AA there was no change in adhesion with pH. Surface zeta potential and contact angle measurements indicate that an increase in pH led to a decrease in surface energy as well as a larger negative surface charge density. Both observations are consistent with deprotonation of the acrylic acid at the PSA-water interface.

Lower initial contact area at high pH could also be explained by an increase in electrostatic repulsion with pH. We also estimated the pKa of the PSA containing 5% AA to be 8.7 ± 0.2. Bulk rheological measurements of the PSA containing AA did not show a significant change in the loss and storage moduli upon exposure to solution between pH3 and pH11. While most of the decrease in adhesion due to the increase in solution pH could be attributed to a change in surface properties, our measurements also indicate that a small change in the bulk properties of the PSAs could also occur as the pH increases, possibly due to the disruption of hydrogen bonding within the PSA.

Supporting information available

Supporting information details: (1) Schematic of PSA and probe surface chemistry; (2) typical debonding force curve; (3) system compliance analysis; (4) determination of surface pKa from receding contact angle measurements; (5) surface energy; (6) work of adhesion; (7) surface zeta potential; (8) double layer forces calculations (9) *in situ* surface fingering wavelength analysis.

Conflict of interest statement

The authors declare the following competing financial interest(s): Two of the co-authors are employees of 3M and this work was partially funded by 3M.

Acknowledgements

This work was supported by 3M and by the National Science Foundation through NSF-CMMI 1728082. We would also like to acknowledge Michael Bevan for access to the surface zeta potential measurements and Sharon Gerecht for access to the rheometer.

References

1. Czech, Z.; Kowalczyk, A.; Kabatc, J.; Świderska, J., Photoreactive UV-crosslinkable solvent-free acrylic pressure-sensitive adhesives containing copolymerizable photoinitiators based on benzophenones. *Eur. Polym. J.* **2012,** *48*, 1446-1454.
2. Pizzi, A.; Mittal, K. L., *Handbook of adhesive technology, revised and expanded*. CRC press: **2003**.
3. Wang, T.; Lei, C. H.; Dalton, A. B.; Creton, C.; Lin, Y.; Fernando, K. S.; Sun, Y. P.; Ma.nea, M.; Asua, J. M.; Keddie, J. L., Waterborne, nanocomposite pressure-sensitive adhesives with high tack energy, optical transparency, and electrical conductivity. *Adv. Mater.* **2006,** *18*, 2730-2734.

4. Rao, M. D., Recent applications of viscoelastic damping for noise control in automobiles and commercial airplanes. *J. Sound Vib.* **2003,** *262*, 457-474.
5. Ahn, B. K.; Kraft, S.; Wang, D.; Sun, X. S., Thermally stable, transparent, pressure-sensitive adhesives from epoxidized and dihydroxyl soybean oil. *Biomacromolecules* **2011,** *12*, 1839-1843.
6. Creton, C., Pressure-sensitive adhesives: an introductory course. *MRS Bull.* **2011,** *28*, 434-439.
7. Wang, T.; Canetta, E.; Weerakkody, T. G.; Keddie, J. L., pH dependence of the properties of waterborne pressure-sensitive adhesives containing acrylic acid. *ACS Appl. Mater. Interfaces.* **2009,** *1*, 631-639.
8. Gurney, R. S.; Morse, A.; Siband, E.; Dupin, D.; Armes, S. P.; Keddie, J. L., Mechanical properties of a waterborne pressure-sensitive adhesive with a percolating poly (acrylic acid)-based diblock copolymer network: Effect of pH. *J. Colloid Interface Sci.* **2015,** *448*, 8-16.
9. Lakrout, H.; Sergot, P.; Creton, C., Direct observation of cavitation and fibrillation in a probe tack experiment on model acrylic pressure-sensitive-adhesives. *J. Adhes.* **1999,** *69*, 307-359.
10. Israelachvili, J. N., *Intermolecular and surface forces*. Academic press: **2011**.
11. Tan, H. S.; Pfister, W. R., Pressure-sensitive adhesives for transdermal drug delivery systems. *Pharm Sci. Technolo. Today* **1999,** *2*, 60-69.
12. Huang, X.; Zhu, Y.; Zhang, X.; Bao, Z.; Lei, D. Y.; Yu, W.; Dai, J.; Wang, Y., Clam-inspired nanoparticle immobilization method using adhesive tape as microchip substrate. *Sens. Actuators B Chem.* **2016,** *222*, 106-111.
13. Kandasamy, R.; Cui, F.; Townsend, N.; Foo, C. C.; Guo, J.; Shenoi, A.; Xiong, Y., A review of vibration control methods for marine offshore structures. *Ocean Eng.* **2016,** *127*, 279-297.
14. Lindner, A.; Lestriez, B.; Mariot, S.; Creton, C.; Maevis, T.; Lühmann, B.; Brummer, R., Adhesive and rheological properties of lightly crosslinked model acrylic networks. *J. Adhes.* **2006,** *82*, 267-310.
15. Creton, C.; Ciccotti, M., Fracture and adhesion of soft materials: a review. *Rep. Prog. Phys.* **2016,** *79*, 046601.
16. Czech, Z., Synthesis and cross-linking of acrylic PSA systems. *J. Adhes. Sci. Technol.* **2007,** *21*, 625-635.
17. Aubrey, D.; Ginosatis, S., Peel adhesion behaviour of carboxylic elastomers. *J. Adhes.* **1981,** *12*, 189-198.
18. Karnal, P.; Roberts, P.; Gryska, S.; King, C.; Barrios, C.; Frechette, J., Importance of substrate functionality on the adhesion and debonding of a pressure sensitive adhesive under water. *ACS Appl. Mater. Interfaces.* **2017**, 42344–42353.
19. Defante, A. P.; Burai, T. N.; Becker, M. L.; Dhinojwala, A., Consequences of water between two hydrophobic surfaces on adhesion and wetting. *Langmuir* **2015,** *31*, 2398-2406.
20. Wang, Y.; Pilkington, G. A.; Dhong, C.; Frechette, J., Elastic deformation during dynamic force measurements in viscous fluids. *Curr. Opin. Colloid Interface Sci.* **2017,** *27*, 43-49.
21. Wang, Y.; Frechette, J., Morphology of soft and rough contact via fluid drainage. *Soft Matter* **2018,** *14*, 7605-7614.
22. Wilhelm, K. P.; Cua, A. B.; Maibach, H. I., Skin aging: effect on transepidermal water loss, stratum corneum hydration, skin surface pH, and casual sebum content. *Arch. Dermatol.* **1991,** *127*, 1806-1809.
23. Bijman, J.; Quinton, P. M., Lactate and bicarbonate uptake in the sweat duct of cystic fibrosis and normal subjects. *Pediatr. Res.* **1987,** *21*, 79.

24. Humphrey, S. P.; Williamson, R. T., A review of saliva: normal composition, flow, and function. *J. Prosthet. Dent.* **2001,** *85*, 162-169.
25. Ibekwe, V. C.; Fadda, H. M.; McConnell, E. L.; Khela, M. K.; Evans, D. F.; Basit, A. W., Interplay between intestinal pH, transit time and feed status on the in vivo performance of pH responsive ileo-colonic release systems. *Pharm. Res.* **2008,** *25*, 1828-1835.
26. Long, F.; Nutting, G.; Harkins, W. D., The surface tension of aqueous soap solutions as a function of hydrogen ion (pH) and salt concentration. I. Sodium laurate and sodium nonylate. *J. Am. Chem. Soc* **1937,** *59*, 2197-2203.
27. Ginn, M.; Noyes, C.; Jungermann, E., The contact angle of water on viable human skin. *J. Colloid Interface Sci.* **1968,** *26*, 146-151.
28. Schindler, M.; Koller, M.; Müller-Buschbaum, P., Pressure-sensitive adhesives under the influence of relative humidity: Inner structure and failure mechanisms. *ACS Appl. Mater. Interfaces.* **2014,** *7*, 12319-12327.
29. Roy, S.; Freiberg, S.; Leblanc, C.; Hore, D. K., Surface structure of acrylate polymer adhesives. *Langmuir* **2017,** *33*, 1763-1768.
30. Hu, K.; Bard, A. J., Use of atomic force microscopy for the study of surface acid− base properties of carboxylic acid-terminated self-assembled monolayers. *Langmuir* **1997,** *13*, 5114-5119.
31. Christendat, D.; Abraham, T.; Xu, Z.; Masliyah, J., Adhesion forces between functionalized probes and hydrophilic silica surfaces. *J. Adhes. Sci. Technol.* **2005,** *19*, 149-163.
32. Vezenov, D. V.; Noy, A.; Rozsnyai, L. F.; Lieber, C. M., Force titrations and ionization state sensitive imaging of functional groups in aqueous solutions by chemical force microscopy. *J. Am. Chem. Soc* **1997,** *119*, 2006-2015.
33. Czech, Z., 2-Ethylhexyl acrylate/4-acryloyloxy benzophenone copolymers as UV-crosslinkable pressure-sensitive adhesives. *Polym. Bull.* **2004,** *52*, 283-288.
34. Roberts, P.; Pilkington, G. A.; Wang, Y.; Frechette, J., A multifunctional force microscope for soft matter with in situ imaging. *Rev. Sci. Instrum.* **2018,** *89*, 043902.
35. Beattie, J. K.; Djerdjev, A. M.; Gray-Weale, A.; Kallay, N.; Lützenkirchen, J.; Preočanin, T.; Selmani, A., pH and the surface tension of water. *J. Colloid Interface Sci.* **2014,** *422*, 54-57.
36. Fowkes, F. M., Attractive Forces at Interfaces. *Ind. Eng. Chem.* **1964,** *56*, 40-52.
37. Van Oss, C. J.; Giese, R. F.; Li, Z.; Murphy, K.; Norris, J.; Chaudhury, M. K.; Good, R. J., Determination of contact angles and pore sizes of porous media by column and thin layer wicking. *J. Adhes. Sci. Technol.* **1992,** *6*, 413-428.
38. Corbett, J. C.; McNeil-Watson, F.; Jack, R. O.; Howarth, M., Measuring surface zeta potential using phase analysis light scattering in a simple dip cell arrangement. *Colloids Surf. A Physicochem. Eng. Asp.* **2012,** *396*, 169-176.
39. Tsavalas, J. G.; Sundberg, D. C., Hydroplasticization of polymers: model predictions and application to emulsion polymers. *Langmuir* **2010,** *26*, 6960-6966.
40. Xiao, Q.; Liu, Y.; Guo, Z.; Liu, Z.; Lohse, D.; Zhang, X., Solvent exchange leading to nanobubble nucleation: A molecular dynamics study. *Langmuir* **2017,** *33*, 8090-8096.
41. Ishida, N.; Sakamoto, M.; Miyahara, M.; Higashitani, K., Attraction between hydrophobic surfaces with and without gas phase. *Langmuir* **2000,** *16*, 5681-5687.
42. Davis, C. S.; Lemoine, F.; Darnige, T.; Martina, D.; Creton, C.; Lindner, A., Debonding mechanisms of soft materials at short contact times. *Langmuir* **2014,** *30*, 10626-10636.
43. Creton, C.; Leibler, L., How does tack depend on time of contact and contact pressure? *J. Polym. Sci. B* **1996,** *34*, 545-554.

44. Beattie, J. K., The intrinsic charge on hydrophobic microfluidic substrates. *Lab Chip.* **2006,** *6*, 1409-1411.
45. Zimmermann, R.; Dukhin, S.; Werner, C., Electrokinetic measurements reveal interfacial charge at polymer films caused by simple electrolyte ions. *J. Phys. Chem. B* **2001,** *105*, 8544-8549.
46. Zimmermann, R.; Norde, W.; Cohen Stuart, M. A.; Werner, C., Electrokinetic characterization of poly (acrylic acid) and poly (ethylene oxide) brushes in aqueous electrolyte solutions. *Langmuir* **2005,** *21*, 5108-5114.
47. Hunter, R. J., *Zeta potential in colloid science: principles and applications*. Academic press: **2013**; Vol. 2.
48. Frechette, J.; Vanderlick, T. K., Making, breaking, and shaping contacts by controlling double layer forces. *Ind. Eng. Chem. Res.* **2008,** *48*, 2315-2319.
49. Roman, B.; Bico, J., Elasto-capillarity: deforming an elastic structure with a liquid droplet. *J. Phys. Condens. Matter* **2010,** *22*, 493101.
50. Style, R. W.; Jagota, A.; Hui, C. Y.; Dufresne, E. R., Elastocapillarity: Surface tension and the mechanics of soft solids. *Annu. Rev. Condens. Matter Phys.* **2017,** *8*, 99-118.
51. Godínez, L. A.; Castro, R.; Kaifer, A. E., Adsorption of viologen-based polyelectrolytes on carboxylate-terminated self-assembled monolayers. *Langmuir* **1996,** *12*, 5087-5092.
52. Fears, K. P.; Creager, S. E.; Latour, R. A., Determination of the surface pK of carboxylic-and amine-terminated alkanethiols using surface plasmon resonance spectroscopy. *Langmuir* **2008,** *24*, 837-843.
53. Bain, C. D.; Whitesides, G. M., A study by contact angle of the acid-base behavior of monolayers containing. omega.-mercaptocarboxylic acids adsorbed on gold: an example of reactive spreading. *Langmuir* **1989,** *5*, 1370-1378.
54. Urry, D.; Gowda, D.; Peng, S.; Parker, T.; Harris, R., Design at nanometric dimensions to enhance hydrophobicity-induced pKa shifts. *J. Am. Chem. Soc* **1992,** *114*, 8716-8717.
55. Wasserman, S. R.; Tao, Y. T.; Whitesides, G. M., Structure and reactivity of alkylsiloxane monolayers formed by reaction of alkyltrichlorosilanes on silicon substrates. *Langmuir* **1989,** *5*, 1074-1087.
56. Owens, D. K.; Wendt, R., Estimation of the surface free energy of polymers. *J. Appl. Polym. Sci.* **1969,** *13*, 1741-1747.
57. Żenkiewicz, M., Methods for the calculation of surface free energy of solids. *J. Achiev. Mater. Manuf. Eng.* **2007,** *24*, 137-145.
58. Falsafi, A.; Tirrell, M.; Pocius, A. V., Compositional effects on the adhesion of acrylic pressure sensitive adhesives. *Langmuir* **2000,** *16*, 1816-1824.
59. Joanny, J.; De Gennes, P. G., A model for contact angle hysteresis. *J. Chem. Phys.* **1984,** *81*, 552-562.
60. Nase, J.; Lindner, A.; Creton, C., Pattern formation during deformation of a confined viscoelastic layer: From a viscous liquid to a soft elastic solid. *Phys. Rev. Lett.* **2008,** *101*, 074503.
61. Janssen, D.; De Palma, R.; Verlaak, S.; Heremans, P.; Dehaen, W., Static solvent contact angle measurements, surface free energy and wettability determination of various self-assembled monolayers on silicon dioxide. *Thin Solid Films* **2006,** *515*, 1433-1438.
62. Zosel, A., Adhesion and tack of polymers: Influence of mechanical properties and surface tensions. *Colloid Polym. Sci.* **1985,** *263*, 541-553.

63. Gent, A., Adhesion and strength of viscoelastic solids. Is there a relationship between adhesion and bulk properties? *Langmuir* **1996,** *12*, 4492-4496.
64. Shanahan, M.; Carre, A., Viscoelastic dissipation in wetting and adhesion phenomena. *Langmuir* **1995,** *11*, 1396-1402.
65. Ahn, D.; Shull, K. R., Effects of methylation and neutralization of carboxylated poly (n-butyl acrylate) on the interfacial and bulk contributions to adhesion. *Langmuir* **1998,** *14*, 3637-3645.
66. Gold, B. J.; Hövelmann, C. H.; Weiss, C.; Radulescu, A.; Allgaier, J.; Pyckhout-Hintzen, W.; Wischnewski, A.; Richter, D., Sacrificial bonds enhance toughness of dual polybutadiene networks. *Polymer* **2016,** *87*, 123-128.
67. Luo, M.-C.; Zeng, J.; Fu, X.; Huang, G.; Wu, J., Toughening diene elastomers by strong hydrogen bond interactions. *Polymer* **2016,** *106*, 21-28.